ISIJ International, Vol. 54 (2014), No. 11, pp. 2643–2648

Anomalous Segregation Kinetics of Phosphorus and Carbon Governed by Carbide Reactions in 2.25Cr-1.5W Heat-resistant Steel

Hyun Je SUNG, Nam Hoe HEO,* Yoon-Uk HEO and Sung-Joon KIM

Graduate Institute of Ferrous Technology, POSTECH, 77 Cheongam, Pohang, 790-784 Republic of Korea.

(*Received on April 28, 2014; accepted on July 23, 2014*)

In a 2.25Cr-1.5W heat-resistant steel containing V and Nb, the formation sequence of carbides are detailed. Such carbide reactions determine directly the anomalous segregation kinetics of phosphorus and carbon at the grain boundary/carbide interface. The anomalous segregation kinetics of phosphorus consists of two maximum segregation peaks and one minimum peak corresponding to the high segregation concentration of carbon. The roles of the carbide reactions on the anomalous segregation kinetics of the solutes are fully understood from the viewpoint of the dissolution of unstable carbides into the matrix for forming the stable carbides, the active segregation of the dissolved carbon into the newly formed carbide interface for the growth and the resultant repulsive segregation between carbon and phosphorus.

KEY WORDS: segregation kinetics; AES; carbides; interface energy; heat-resistant steel.

1. Introduction

The driving force for segregation of a solute to interfaces of an alloy system is composed of two components: the elastic strain energy arising from the atomic size difference between the solvent and the solute and the decrease in interface energy which results from the segregation of the solute.[1,2] The equilibrium segregation concentration increases with decreasing temperature due to the increase in elastic strain energy and with increasing bulk content of the solute.[2,3] In case of no precipitation reactions related to the segregant, the segregation concentration increases gradually with increasing time at a temperature, and it is finally saturated with further increasing time to the equilibrium segregation concentration at the temperature. However, if a precipitation reaction directly related to the segregant occurs, the segregation kinetics is greatly influenced by the precipitation reaction.[4,5]

Meanwhile, it was suggested in CrMoV heat-resistant steels containing several hundred ppm of phosphorus that the decrease in grain boundary segregation concentration of phosphorus after a maximum concentration during long-term aging in the temperature range of 480–530°C is related to intermetallic quasi-crystals containing phosphorus which are formed at grain boundaries and the surface of pre-formed $M_{23}C_6$ carbides,[6–10] or that it is due to the formation at the grain boundaries of M_6C carbides containing molybdenum, iron and phosphorus.[11] Recently, it was also proposed that the anomalous segregation behavior of solutes (especially, P, C and Cr) were deeply related to the dissolution of pre-formed carbides into the matrix without any clear evidence.[12]

Irrespective of the explanations mentioned above, the anomalous segregation behavior of the solutes observed in heat-resistant steels is not still clearly understood. In this study, the carbide reactions occurring in a heat-resistant steel are detailed and they are correlated to the anomalous segregation behaviors of the solutes.

2. Experimental Procedure

A 2.25Cr-1.5W steel ingot was prepared using a vacuum induction melting. The chemical composition of the steel is shown in **Table 1**. The ingot was homogenized at 1 150°C for 7.2 ks and subsequently hot-rolled to 12 mm thick plates. Un-notched and cylindrical specimens for stress rupture tests, which have a gage length of 15 mm and a gauge diameter of 6 mm, were machined from the plates in the hot-rolling direction. In order to investigate the carbide reactions and the segregation behavior of solutes (especially, C and P) from the initial stage of the rupture test, the specimens were austenitized at 1 050°C for 3.6 ks under a vacuum of about 1 Pa and water-quenched. A full martensitic structure was obtained after water-quenching. The stress rupture test was performed at 700°C in the tensile stress range of 75 to 300 MPa, using conventional creep testers (ATS Ltd., USA). **Table 2** shows the rupture time for each case of tensile stresses at 700°C. The rupture test specimens to which an N-type thermocouple was attached were heated from room temperature to the test temperature at a heating rate of 1 200°C/h. The rupture test was carried out without

* Corresponding author: E-mail: nhheo@postech.ac.kr
DOI: http://dx.doi.org/10.2355/isijinternational.54.2643

Table 1. The chemical composition of the prepared steel (wt%).

C	Si	Mn	P	S	Cr	V	Nb	Ti	W	N	Fe
0.13	0.35	0.5	0.060	0.002	2.28	0.24	0.047	0.006	1.48	0.009	Balance

Table 2. The rupture time of specimens for each of tensile stresses at 700°C.[12)]

Tensile stress (MPa)	300	275	250	225	200	150	125	100	75
Time to rupture (second)	300	600	1 320	2 160	3 780	13 800	22 920	51 960	179 160

soaking at the test temperature. Kinds of carbides at each stage and their composition and morphology were investigated, using a carbon extraction replica method and an energy-dispersive spectroscope (EDS) attached to a field emission transmission electron microscope (JEM-2100F, Japan Electronic Optics Ltd., Tokyo, Japan). The interfacial segregation of solutes was investigated, using an Auger electron spectroscope (AES, PHI 700, Japan). The AES specimens machined from the ruptured specimens in the tensile stress direction were chilled in the AES with liquid nitrogen for 3.6 ks and *in-situ* fractured in an ultra-high vacuum of 9×10^{-8} Pa or better. Typical parameters were the primary electron beam energy of 3 keV and an electron beam size of about 200 nm. In investigating the segregation behaviors of solutes, the AES results of the present study have been obtained from the grain boundary surface side among the prior austenite grain boundary/carbide interface of intergranular-fractured AES specimens in which the carbides are absent. The interfaces of about 10 points were chosen for the AES analysis of each specimen. The AES peaks used were Fe_{703}, P_{120} and C_{271}, and the peak-height-ratios (I/I_{Fe}) obtained from the differential AES spectra were averaged.

3. Results and Discussion

3.1. Anomalous Segregation Kinetics of Solutes Occurring during Rupture Test and Various Kinds of Carbide Reactions

As shown in **Fig. 1**, the intergranular fracture surface is generally composed of carbide-free grain boundaries and grain boundary/carbide interfaces that carbides resided.[12–14)] The elevated temperature intergranular cracking occurs initially at the grain boundary/carbide interfaces showing the segregation concentration of phosphorus higher than that of the carbide-free grain boundaries. The decohesion at the carbide-free grain boundaries follows finally the initial cracking. **Figure 2** shows the anomalous segregation kinetics of phosphorus and carbon at grain boundary/carbide interfaces. This was obtained through the correction of the experimental errors made in a previous research.[12)] That is, the previous research showed that the segregation concentration of phosphorus increased with further increasing time after the minimum peak and it was saturated to a high concentration. Unlike the equilibrium segregation kinetics,[2,3)] the profile of phosphorus segregation concentration in Fig. 2 shows two maximum peaks and one minimum peak in a time to failure versus segregation concentration plot. Two maximum peaks of phosphorus correspond to the very low segregation concentration of carbon. In addition, the minimum peak of

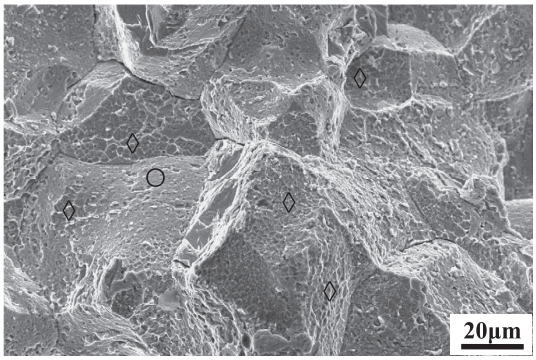

Fig. 1. Fracture surface[12)] of AES specimen which is composed of carbide-free grain boundaries (○) and grain boundary/carbide interfaces (◇) that the carbides resided. The specimen corresponds to the condition of 200 MPa in Table 2.

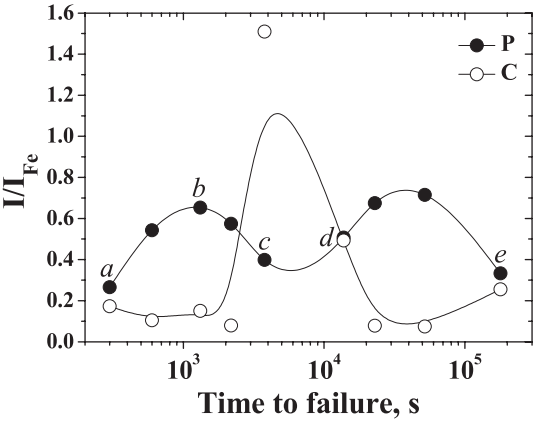

Fig. 2. The anomalous segregation kinetics of phosphorus and carbon at grain boundary/carbide interfaces that carbides resided.

phosphorus corresponds to the strong carbon peak, which is named as the repulsive segregation between carbon and phosphorus.[15)] In order to investigate the correlation between the anomalous segregation kinetics of the solutes and the carbide reactions, the equilibrium phase fractions in the present steel were calculated, and carbides existing in specimens ruptured at stages of *a*, *b*, *c*, *d* and *e* of Fig. 2 were analyzed.

Figure 3 shows the equilibrium phase fractions which were calculated by Thermo-Calc software using the TCFE6 database. According to the calculation and the related **Table 3**, carbides of M_6C (M=W, Fe), $M_{23}C_6$ (M=Cr, W, Fe), M_7C_3 (M=Cr, Fe) and MC (M=V, Nb) can be formed during heating to 700°C for the rupture test. Based on the calculation, the additional formation of M_3P (M=Fe, Cr) phosphides is

also expected, but the phases were not observed in the present study. **Figure 4** shows bright field images obtained from the phases at the stage *a* of Fig. 2, the electron diffraction patterns and the EDS analysis results. Phases are mainly composed of Cr-rich M_7C_3 carbides with a trace of unexpected Fe-rich M_3C carbides, both of which are the non-equilibrium phases at 700°C. Both of the M_3C and M_7C_3 carbides show an orthorhombic crystal structure, based on the electron diffraction patterns of Fig. 4. It has been suggested that various types of carbides such as -carbide, M_3C, M_7C_3, $M_{23}C_6$ and M_6C are in turn formed during tempering in Cr-added steels[16–23] and that the carbides are formed through either the independent nucleation in the matrix or the *in-situ* transformation from the pre-existing carbides. Experimentally, it takes about 3.6 ks in heating the creep specimen to the test temperature of 700°C. Because the M_7C_3 carbide nucleated from a M_3C carbide was not observed at the stage *a*, the formation of the M_7C_3 carbides in the present study is attributed to not the *in-situ* transformation from the M_3C carbides. Therefore, the M_7C_3 carbides are directly formed from the supersaturated matrix of solutes in the temperature range of 450–650°C during heating to 700°C or through the dissolution of the pre-formed M_3C carbides into matrix and the subsequent nucleation reaction.

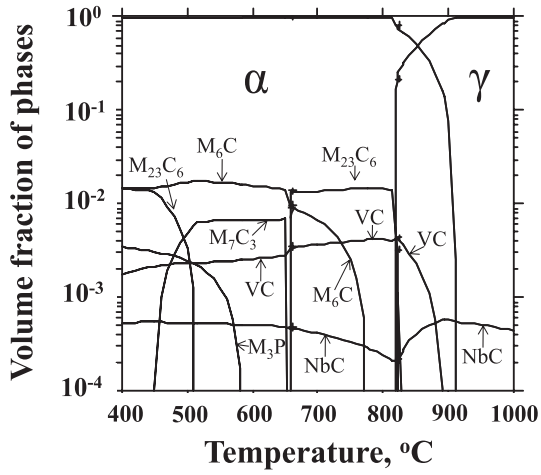

Fig. 3. The equilibrium phase fractions which were calculated by Thermo-Calc software using the TCFE6 database.

Table 3. The mass fraction of alloying elements in equilibrium precipitates calculated by Thermo-Calc software using the TCFE6 database.

	Fe	C	Mn	P	Cr	Nb	Ti	V	W	N
M_6C	0.240	0.017	–	–	0.001	0.001	–	0.016	0.725	–
$M_{23}C_6$	0.140	0.048	0.009	–	0.567	–	–	0.035	0.201	–
M_7C_3	0.173	0.088	0.002	–	0.680	–	–	0.044	0.013	–
VC	0.047	0.153	–	–	0.009	0.005	–	0.720	0.060	0.006
NbC	–	0.120	–	–	0.057	0.777	0.0378	0.008	–	0.0002
M_3P	0.467	–	–	0.160	0.373	–	–	–	–	–

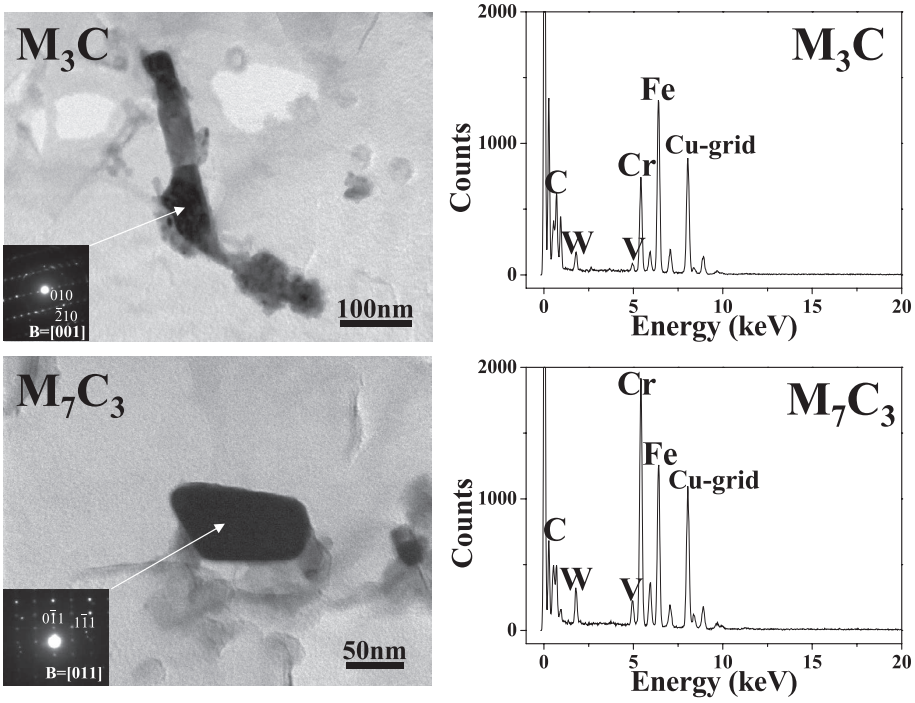

Fig. 4. Bright field images obtained from precipitates of the stage *a* of Fig. 1, the electron diffraction patterns and the EDS analysis results.

Figure 5 shows the bright field image obtained from a precipitate of the stage *b* and the electron diffraction pattern. Without any trace of the M_3C carbides, all the carbides are composed of the Cr-rich M_7C_3 non-equilibrium carbides formed during heating to 700°C. **Figure 6** shows bright field images obtained from precipitates of the stage *c* and the electron diffraction patterns. The Cr-rich equilibrium $M_{23}C_6$ carbides begin to be observed, while the Cr-rich M_7C_3 carbides still remain at the stage *c*. Because the $M_{23}C_6$ carbides formed on the M_7C_3 carbide surface are not observed, the transformation from M_7C_3 to $M_{23}C_6$ also results from the dissolution of the M_7C_3 carbides into the matrix and the subsequent nucleation of the new equilibrium $M_{23}C_6$ carbides. **Figure 7** shows bright field images obtained from precipitates of the stage *d*, the electron diffraction patterns and the EDS analysis results. Additional equilibrium M_6C carbides, which contain tungsten more than the $M_{23}C_6$ carbides, are observed together with the pre-existing $M_{23}C_6$ and M_7C_3 carbides. The EDS result for the M_6C carbides shows a strong Cr peak, which is not consistent with the calculation result of Table 3. Unlike the calculation, the Cr peak from the M_6C carbides was also noticeable even at the stage *e*, although it became weaker than the W peak. **Figure 8** shows bright field images obtained from precipitates of the stage *e*, the electron diffraction patterns and the EDS analysis results. Equilibrium V- or Nb-rich MC carbides are observed in the matrix as well as on the $M_{23}C_6$ carbide surfaces, while the non-equilibrium M_7C_3 carbides disappear completely. Based on Fig. 8(b), the weak Cr peak obtained from the Nb-rich MC carbide surface of Fig. 8(a) is due to the interference effect of the $M_{23}C_6$ carbides just near the MC carbides. The mass fraction of alloying elements in the carbides of Table 3 is roughly consistent with the experimental results of Figs. 4, 7 and 8.

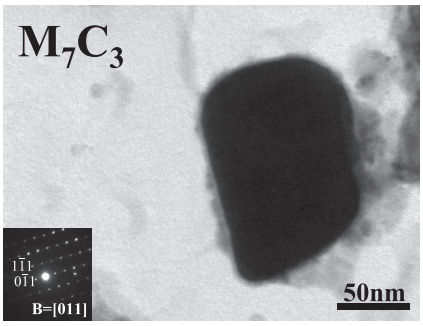

Fig. 5. A bright field image obtained from a precipitate of the stage *b* and the electron diffraction pattern.

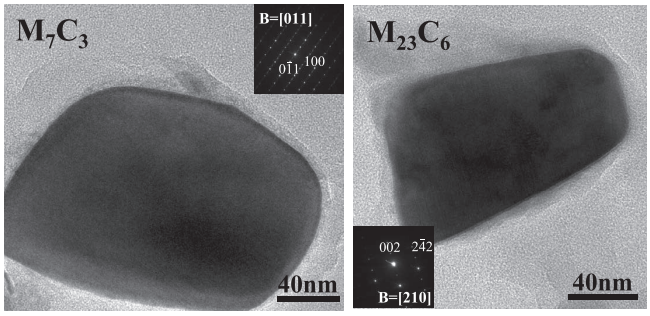

Fig. 6. Bright field images obtained from precipitates of the stage *c* and the electron diffraction patterns.

3.2. Formation Sequence of Carbides

Finally, the formation sequence of carbides in the present steel is 1) the M_3C carbides appearing in the low temperature range at the expense of the supersaturated carbon during heating to the rupture test temperature, 2) the M_7C_3 carbides

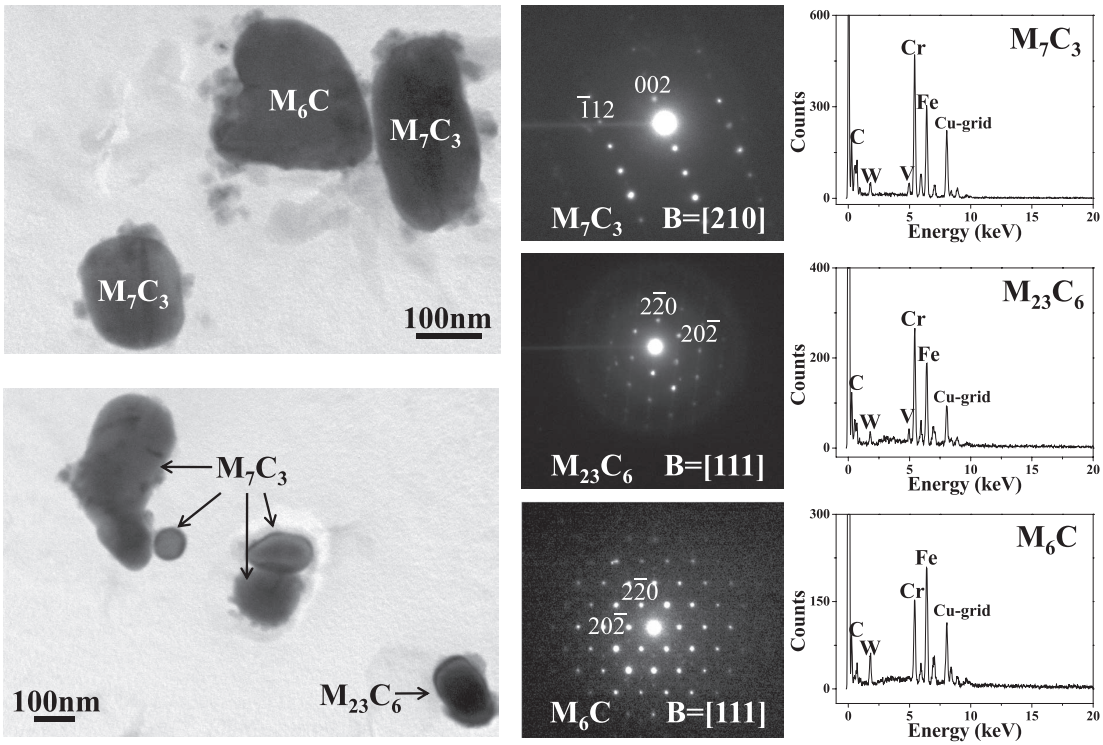

Fig. 7. Bright field images obtained from precipitates of the stage *d*, the electron diffraction patterns and the EDS analysis results.

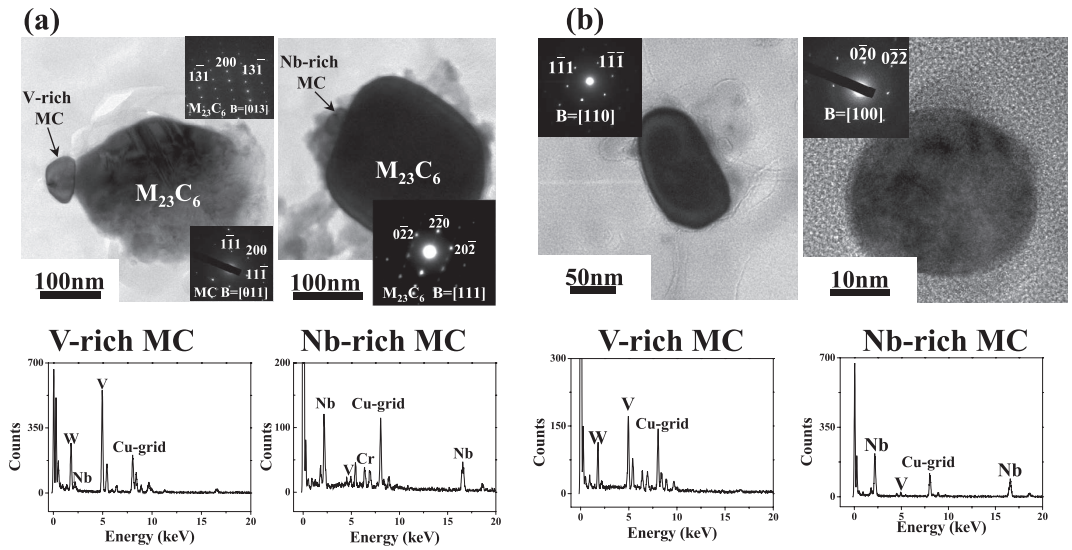

Fig. 8. Bright field images obtained from precipitates of the stage *e*, the electron diffraction patterns and the EDS analysis results: (a) MC on $M_{23}C_6$ and (b) MC in the matrix.

in the relatively high temperature range, 3) the dissolution of the M_3C carbides into the matrix and the additional formation of the M_7C_3 carbides during the time period of the stages *a* and *b* of 700°C, 4) the dissolution of the M_7C_3 carbides into the matrix and the formation of the $M_{23}C_6$ and M_6C carbides during the time period between two maximum peaks of phosphorus, and 5) the final formation of the V- or Nb-rich MC carbides in the matrix as well as on the pre-formed $M_{23}C_6$ carbide surface.

Because the composition of the $M_{23}C_6$ carbides is, as shown in Table 3 and Fig. 7, more similar to that of the M_7C_3 carbides than the M_6C carbides of a high tungsten content, the formation of the $M_{23}C_6$ carbides are easier than the formation of the M_6C carbides during the dissolution of the M_7C_3 carbides into the matrix. The V- and the Nb-rich MC carbides are finally formed due to the similarly low diffusivities of vanadium[24] and niobium.[25] Based on Fig. 8, the V- and the Nb-rich MC carbides are mainly formed through some dissolution of the $M_{23}C_6$ carbides which increases slightly the dissolved carbon content in the matrix.

3.3. Correlation between Carbide Reactions, Interface Energy and Anomalous Segregation Kinetics of Solutes

In order to form the $M_{23}C_6$ and M_6C equilibrium carbides, the non-equilibrium M_7C_3 carbides after the disappearance of the M_3C carbides should be massively dissolved into the matrix. This causes the abrupt increase in the dissolved carbon content of the matrix. As a result, while the equilibrium $M_{23}C_6$ and M_6C carbides are formed at the grain boundaries and in the matrix, the dissolved carbon segregates actively into the grain boundary/newly formed carbide interfaces for the growth of the equilibrium carbides. This results in the drastic increase in segregation concentration of carbon of Fig. 2 and the subsequent decrease in segregation concentration of phosphorus.[15] While the M_3C carbides are dissolved into the matrix in the time period of *a* to *b*, the reason why the segregation concentration of carbon is little changed is attributed to the very low phase fraction of the M_3C carbides. While the equilibrium carbide reactions proceed further, the segregation concentration of carbon at the interface decreases abruptly to a low concentration after the maximum due to the fast decrease in dissolved carbon content. Contrary to such a segregation behavior of carbon, the segregation concentration of phosphorus again increases to the second maximum peak.

On the other hand, the segregation concentration of phosphorus after the second maximum peak decreases rapidly with increasing time, while the segregation concentration of carbon increases gradually. Such segregation behaviors of the solutes can be understood in the light of the dissolution of some amount of the $M_{23}C_6$ or M_6C carbides and the concurrent formation of the equilibrium MC carbides. The low segregation concentration of carbon corresponding to the second maximum peak of phosphorus implies that the dissolution reaction of the non-equilibrium M_7C_3 carbides has been finished. This is also supported by Fig. 8.

Generally, the interface energy in metals decreases initially drastically with increasing interfacial segregation concentration of solutes and gradually with further increasing segregation concentration.[26,27] This means that, because the newly formed carbide interface is the high energy site preferential for the segregation, the solutes segregate actively into the fresh carbide interface in order to minimize the total interface energy. Considering the minimization in total interface area, it is reasonable that the formation of the MC carbides on the pre-formed carbide surface is, as shown in Fig. 8(a), energetically more favorable than that of the carbides in the matrix of Fig. 8(b). As a result, the abrupt decrease in segregation concentration of phosphorus after the second maximum peak can be attributed to two factors: the partitioning effect in **Fig. 9** of the phosphorus pre-segregated on the surface of the $M_{23}C_6$ carbides preferentially formed at the prior austenite grain boundaries onto the interface of MC carbides newly formed on the carbides and the additional slight increase in segregation concentration of carbon. The correlation between the formation sequence of the carbides in the present steel and its effect on the anomalous segregation kinetics of the solutes is finally summarized in **Fig. 10**.

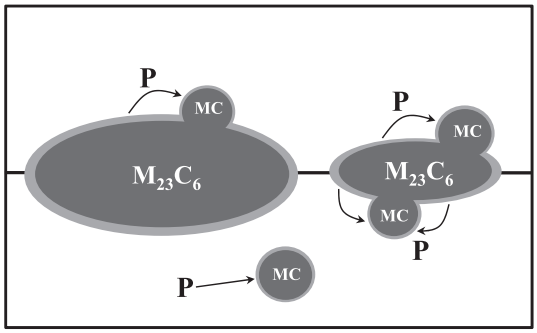

Fig. 9. A schematic diagram explaining the redistribution of pre-segregated phosphorus into the fresh MX phase interface.

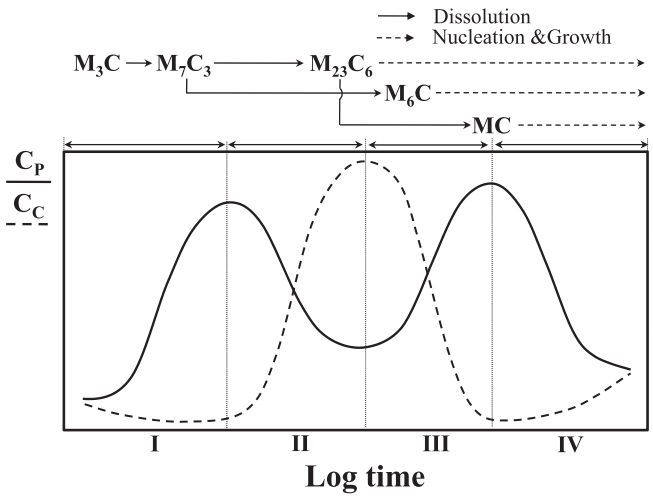

Fig. 10. A schematic diagram for understanding the correlation between carbide reactions and anomalous segregation kinetics of solutes.

4. Summary

The carbides in a 2.25Cr-1.5W heat-resistant steel containing V and Nb are M_3C and M_7C_3 formed during heating to 700°C. The $M_{23}C_6$, M_6C and MC carbides are in turn formed during rupture test at 700°C. Such carbide reactions result in the anomalous segregation kinetics of carbon and phosphorus at the grain boundary/carbide interface. The anomalous segregation kinetics is composed of two maximum segregation peaks of phosphorus and one minimum peak which corresponds to the maximum segregation peak of carbon. The maximum segregation peak of carbon is due to the active segregation of the dissolved carbon into the interface for forming and growing the equilibrium $M_{23}C_6$ and M_6C carbides, which arises from the massive dissolution of the non-equilibrium M_7C_3 carbides into the matrix. The decrease in phosphorus segregation concentration after the second maximum peak is mainly attributed to the partitioning effect of the phosphorus pre-segregated on the surface of the $M_{23}C_6$ carbides onto the interface of MC carbides newly formed on the carbides and the additional segregation of the dissolved carbon to the interface.

Acknowledgment

The authors thank Korea Institute of Energy Technology Evaluation and Planning for the financial support.

REFERENCES

1) J. W. Gibbs: The Scientific Papers of J. W. Gibbs, Vol. 1, Dover Publication Inc., Dover, New York, (1961).
2) D. McLean: Grain Boundaries in Metals, Oxford University Press, London, (1957).
3) E. D. Hondros and M. P. Seah: *Int. Metall. Rev.*, **22** (1977), 262.
4) N. H. Heo: *Acta Metall.*, **44** (1996), 3015.
5) N. H. Heo: *Acta Metall.*, **44** (1996), 1581.
6) J. Janovec, B. Richarz and H. J. Grabke: *Scr. Metall. Mater.*, **33** (1995), 295.
7) J. Janovec, B. Richarz and H. J. Grabke: *Steel Res.*, **65** (1994), 438.
8) M. Hättestrand, M. Schwind and H. O. Adrén: *Mater. Sci. Eng. A*, **250** (1998), 27.
9) P. Hofer, M. K. Miller, S. S. Babu, S. A. David and H. Cerjak: *Metall. Mater. Trans.*, **31** (2000), 975.
10) G. R. Jordan, S. J. Andrews and C. A. Hippsley: *Mater. Sci. Technol.*, **9** (1993), 1115.
11) J. Janovec, A. Výrostkova, P. Sevc, J. S. Robinson, M. Svoboda, J. Kresťanková and H. J. Grabke: *Acta Mater.*, **51** (2003), 4025.
12) N. H. Heo and S.-J. Kim: *Mater. Sci. Eng. A*, **556** (2012), 553.
13) N. H. Heo, J. C. Chang, K. B. Yoo, J. K. Lee and J. Kim: *Mater. Sci. Eng. A*, **528** (2011), 2678.
14) N. H. Heo, J. C. Chang and S.-J. Kim: *Mater. Sci. Eng. A*, **559** (2013), 665.
15) H. J. Grabke: *Steel Res.*, **57** (1986), 178.
16) K. Kuo: *J. Iron Steel Inst.*, **184** (1957), 258.
17) E. Smith and J. Nutting: *J. Iron Steel Inst.*, **187** (1957), 314.
18) F. B. Pickering: *J. Iron Steel Inst.*, **189** (1958), 148.
19) F. Wever and W. Koch: *Stahl Eisen*, **74** (1954), 989.
20) A. K. Seal and R. W. K. Honeycombe: *J. Iron Steel Inst.*, **188** (1985), 9.
21) F. B. Pickering: *ISI Spec. Rep.*, **64** (1959), 118.
22) K. C. Mills, B. B. Argent and A. G. Quarrell: *J. Iron Steel Inst.*, **197** (1961), 9.
23) V. B. Nileshwar and A. G. Quarrell: *ISI Spec. Rep.*, **64** (1959), 259.
24) S. G. Michael and E. F. Morris: *Calphad*, **25** (2001), 207.
25) J. Čermák, J. Růžičková and A. Pokorná: *Scr. Mater.*, **35** (1996), 441.
26) M. P. Seah and E. D. Hondros: *Proc. R. Soc. Lond A*, **335** (1973), 191.
27) E. D. Hondros: Interfaces, Butterworths, London, (1969).